EasyChair Preprint

№ XXX

Design, Control, and Testing of Intelligent Electromagnetic Footwear for Astronautical Applications

Severin Meyer, Joseph A. Paradiso, Daniel Visan Levine, Don Derek Haddad and Irmandy Wicaksono

EasyChair preprints are intended for rapid dissemination of research results and are integrated with the rest of EasyChair.

July 12, 2025

Design, Control, and Testing of Intelligent Electromagnetic Footwear for Astronautical Applications

Severin Meyer[1]*, Daniel V. Levine[2], Don D. Haddad[3], Irmandy Wicaksono[4] and Joseph A. Paradiso[5]
MIT Media Lab, Cambridge, Massachusetts, 02142, USA

This paper revisits a classic concept from science fiction, the electromagnetic shoe. The ability to effortlessly attach, detach, and walk in weightlessness would open up a wide range of quality-of-life improvements for astronauts during their everyday tasks inside upcoming large space habitats. To demonstrate this, a prototype shoe was developed and tested in microgravity under operational conditions on a parabolic flight. The key to the prototype's functionality is for it to be solely controlled by natural human gait movements, allowing the user to walk without needing to focus on the system's actuation. Therefore, the prototype entails a sensor package to measure each foot's dynamics and deformation, allowing for accurate control of the electromagnets on the outside sole of the shoe. The sensor outputs are read and processed by a low-cost and low-power embedded system based around off-the-shelf microcontrollers, offering an extensive range of capabilities to the system that enable different control algorithms and the use of wireless communication between its components. Two control methods are proposed and investigated: a sensor-based state machine and a neural network approach, both running in real time onboard the on-shoe embedded microcontrollers. The system was tested successfully on the ground and during the conducted parabolic flight, providing an assessment of the prototype's performance, power efficiency, and user experience in standard-, low- and microgravity environments.

Acronyms and Nomenclature

AC	=	Alternating Current
ADC	=	Analog-to-Digital Converter
AlNiCo	=	Aluminum Nickel Cobalt
ARM	=	Advanced RISC Machines
DC	=	Direct Current
EM	=	Electromagnetic
EPM	=	Electropermanent Magnet
GPIO	=	General-Purpose Input/Output
IMU	=	Inertial Measurement Unit
IVA	=	Intravehicular Activity
LED	=	Light Emitting Diode
MSU	=	Magnet and Sensor Unit
PSU	=	Power Supply Unit
ReLU	=	Rectified Linear Unit
ROC	=	Receiver Operating Characteristic
SCU	=	Shoe Control Unit
TPU	=	Thermoplastic Polyurethane
UART	=	Universal Asynchronous Receiver/Transmitter

[1] Research Affiliate, MIT Media Lab; M.Sc. Student, ETH Zürich. *sevmeyer@mit.edu
[2] Ph.D. Candidate/Research Assistant, MIT Media Lab.
[3] Planetary Science Software Engineer, NASA Ames Research Center, MIT Space Exploration Initiative.
[4] Assistant Professor, Division of Industrial Design, National University of Singapore.
[5] Alexander W. Dreyfoos (1954) Professor of Media Arts and Sciences, MIT Media Lab.

I. Introduction

WITH today's fast-paced advancements in launch capabilities, the price per kilogram of mass sent to earth orbit has steadily fallen in recent years and is projected to drastically decrease further in the coming decades[1]. This circumstance, in combination with new innovations in space architecture, such as proposed self-assembling space stations, inflatable habitats, and the use of larger vehicles, will significantly increase the pressurized volumes available to future astronauts[2,3]. This calls for all current concepts of living and working in space to be analyzed and adapted to this new environment, including IVA locomotion.

This paper revisits a classic idea from science fiction and aims to bring it into the 21st century: footwear as a dynamic tethering system, made popular through the movie *2001: A Space Odyssey*, where astronauts use *Velcro*-based shoes to walk naturally in microgravity[4]. In more recent lore, such as *The Expanse*, electromagnets are often chosen as the attachment mechanism that offers advantages, such as the ability to turn the attachment force on and off on command[5]. Advancements and cost reductions in key areas such as sensor technology, embedded systems, energy storage devices, and electromagnets have made a compact and affordable design of such a system now more feasible than ever.

In 2022, researchers at *MIT Media Lab* conducted a parabolic flight experiment to test a prototype of an electromagnetic space shoe[6]. This proof-of-concept device, known as the *Space Grip Shoe*, aimed to explore practical applications of magnetic locomotion in microgravity. The prototype operated on a simple, user-controlled system where electromagnets embedded in the sole could be manually toggled on and off via a switch. The goal of this technology is to allow astronauts to move and stabilize themselves without occupying their hands, unlike most traditional tethering methods, thereby freeing their attention and capabilities for more critical tasks. However, further work is required to fully realize this goal.

This paper aims to develop a next generation prototype that meets the project requirements as defined in the system development and design section, implement an innovative state-of-the-art control algorithm, test the system in an operational environment, and show the functionality of the prototype through a quantitative and qualitative analysis of the data gathered.

II. Background and Related Work

Recent advancements in wearable technologies have continually evolved to enhance the safety and efficiency of astronauts' daily activities in space. Given the extreme conditions present, such as microgravity, radiation exposure, and drastic temperature variations, highly specialized wearable equipment is essential for astronaut well-being and performance[7]. As an example, spacesuits and gloves have seen significant innovations, integrating compression technology to maintain circulation, physiological sensing for real-time health monitoring, tactile feedback to enhance dexterity, thermoregulation for temperature control, and exoskeletons to support movement and reduce fatigue[8,9,10,11,12]. These advancements ensure that astronauts can perform their tasks with greater efficiency and reduced risk of injury while adapting to the challenges posed by space environments.

In a microgravity environment, conventional shoes lose their primary role of providing traction and support, necessitating alternative designs to ensure stability and secure movement for astronauts.

One of the earliest known efforts in this field was the development of magnetic boots for astronauts in the 1960s by engineer *Raymond Radus*[13]. These boots, referred to as *Radus Boots*, introduced a novel mechanism for automatically switching permanent magnetic fields, enabling astronauts to achieve a slow but steady walking motion[14].

In 1969, *A.W. Hanger* and *A.A. Rosener* authored a technical report titled *Final Analysis/Design and Prototype Construction of a Selected Mobility and Restraint Device* for *Martin Marietta* under the auspices of *NASA*[15]. This report addressed the necessity for effective mobility and restraint mechanisms within larger spacecraft, aiming to assist crew members in performing tasks in microgravity environments. The study encompassed the analysis, design, and prototype development of footwear with integrated permanent magnets, described as shufflers according to the method of locomotion used while wearing them, tailored to enhance astronaut mobility and stability during missions[16]. Permanent magnets offer a simple and low-cost solution to this design challenge but lead to some drawbacks: The gait pattern is far from natural and resembles more of a shuffling motion. If proper footsteps are to be taken the shoes user needs to manually overcome the magnetic force which can become strenuous over longer periods of time. In an ideal case, the deployed system should provide gait close to walking under standard gravity to optimize the user experience.

In 1973, during the *Skylab II* missions, the first U.S. space station, *NASA* introduced another unique approach to astronaut footwear[9]. The specialized shoes developed for this mission featured triangular cleats on the outsole, allowing them to lock onto a metallic grid surface and provide a stable foothold. This innovation was designed to enhance astronaut mobility and stability in a microgravity environment.

Despite these efforts, research into space footwear has remained limited, leaving room for future technological advancements that could revolutionize astronaut movement and comfort in microgravity environments. Astronauts have continued to rely on simpler solutions such as conventional tethers and foot straps to maintain their positions during missions. Additionally, *Velcro* has played a fundamental role in space operations, helping astronauts secure themselves, their tools, and other essential objects. The hook-and-loop fastening system has been widely applied to gloves, suits, and the interior surfaces of spacecraft, allowing astronauts and their tools to remain in place while working.

III. System Development and Design

For the proposed electromagnetic footwear, three different scenarios are key to its functionality: walking, standing, and sitting. The transitions between the different states need to be considered as well to mitigate failure modes. Walking, due to its dynamic nature, is the most difficult to implement and will be the focus of this paper. The magnetic system on the shoe needs to change its properties constantly to attach or release the feet correctly at a given point in time. When considering a single foot, three phases in the human gait cycle can be identified, where different scenarios in terms of ground contact are present, as illustrated in Figure 1. These scenarios dictate the necessary actuation of the attachment system, and it is crucial for the prototype to detect and classify these different gait phases correctly:

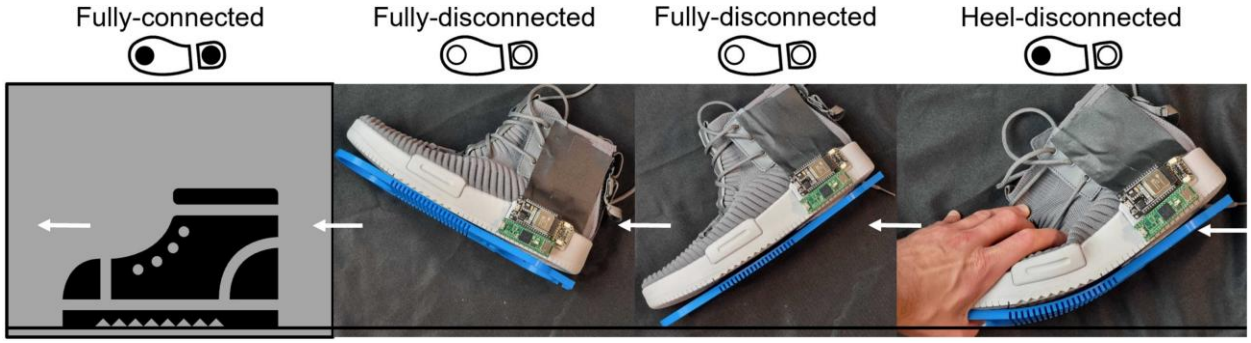

Figure 1: Gait phases with ground-contact scenarios

1) **Heel-disconnected:** The first motion, when starting to walk, is not to immediately lift the whole foot, but rather to push the heel up. Only when a certain angle between the back foot's sole and the ground is reached does the frontal part of the foot release fully. This motion is critical in the gait phase since it allows for naturally pushing the body forward rather than just upwards.
2) **Fully-disconnected:** When the heel is pushed up sufficiently, the foot starts losing contact with the ground and begins the swing phase. Here, the leg is rotating forward while the foot is changing its angle around the ankle such that the heel can strike the ground correctly.
3) **Fully-connected:** The moment the heel touches the ground, the fully-connected phase commences. This phase is traditionally split into heel strike and stance phases for gait analysis[17,18]. Still, for the presented use case, they can be combined due to the activation of the electromagnetic system supporting the natural progression between the two phases, simplifying the control task.

A. System Requirements

1) The power system shall be self-monitoring and able to assess the state of the battery to prevent damage.
2) There shall be a mechanism to release the user from the ground through a safety switch.
3) The system shall prevent the user from being fully released from the ground, without their authorization.
4) The system shall be fully gait-controlled without any additional inputs.
5) The integrated power source shall be able to power the system for at least 30 min.
6) The system shall always provide an attachment force to the ground of at least 400 N.
7) The system shall run with a response time of no more than 20 ms and a sampling rate of no less than 50 Hz.
8) The system shall be compliant with all requirements set by the parabolic flight provider.

In this paper, the system is envisioned to only be used during IVA due to the complexity and safety redundancies necessary to qualify such a locomotion system outside of spacecraft, originating from the inherent risk of disconnecting through possible single points of failure in the system.
Requirement 5 originates from the experience of flyers of previous parabola flights. With an expected number of 20 parabolas flown, each with a low-gravity phase of up to 30 s, the required time the system needs to be powered on can be estimated to be 10 min at minimum. With a prototype able to turn on and off, 30 minutes of battery life is more than sufficient for our tests and includes a substantial safety buffer. Actual operational requirements will most likely require a longer lifetime, necessitating design improvements such as the use of electropermanent magnets.

The attachment force needed, defined by requirement 6, was determined experimentally: An IMU was mounted near the center of mass of a person conducting everyday movements, such as standing up and sitting down, and the total acceleration was measured. Knowing force equals mass times acceleration, the body mass can be multiplied by the accelerations measured after subtracting Earth's gravitational acceleration of 1 g, and the force necessary to hold the person on the ground can be estimated. Having measured a maximum acceleration of 0.5 g and considering a person weighing 80 kg, the requirement for the holding force can be set to 400 N. This is a conservative estimation, due to the fast pace of the movements conducted. Movements in microgravity become much slower and more graceful, only requiring a fraction of the holding force as measured during the conducted IMU test[19].

The defined response time of 20 ms and sampling frequency of 50 Hz, called for in requirement 7 originates from research of machine learning algorithms for gait deformity detection[20]. Below a certain sampling rate, essential aspects of the gait cycle cannot be measured[21].

Systems deployed on actual space missions must function in a highly complex and demanding environment with numerous interactions with other components. This paper aims to develop a first prototype and proof of concept, fulfilling the main testbed requirements listed above.

B. System Overview and Interfaces

The designed system consists of a PSU (Power Supply Unit), as well as a left and right shoe, each made up of a SCU (Shoe Control Unit) and MSU (Magnet and Sensor Unit). The subsystems of the prototype can be seen illustrated in Figure 2. Their purpose, tasks, and interfaces are defined as follows:

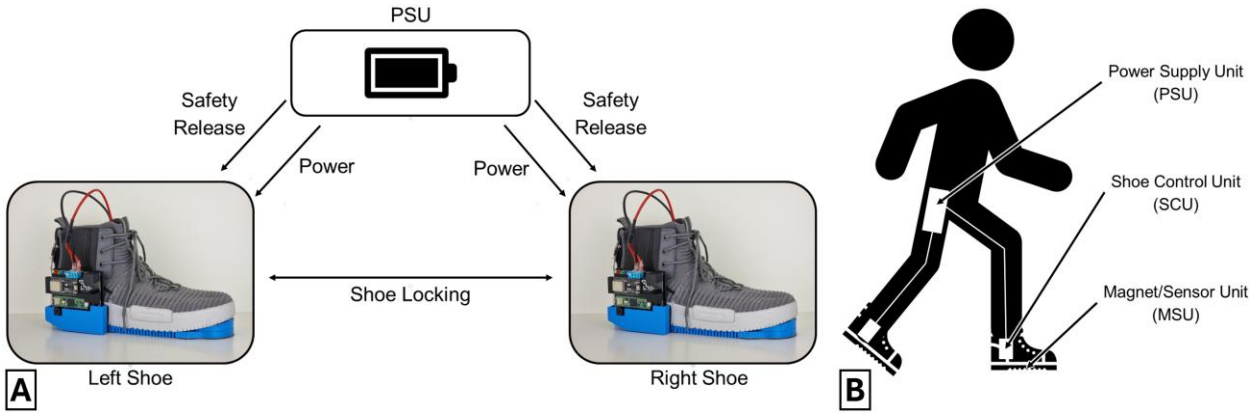

Figure 2: A) Subsystem interfaces, B) System overview

1) **PSU:** The power supply unit's main tasks are to supply both shoes with power and to monitor the battery. It furthermore provides a way for the user to interact with the system, such as turning it on and off, as well as deactivating all magnets by means of a safety switch, such that both feet can be released from the ground.
2) **SCU:** The shoe control unit's tasks are to sample all sensors of the MSU, process the incoming data, and finally save everything on a data storage device. Meanwhile, it needs to feed the sensor data into a control algorithm that outputs the necessary actuation commands for the electromagnets. The SCU also needs to facilitate the capability of communicating with the SCU of the second shoe wirelessly, such that critical information can be passed back and forth. These tasks need to be completed within a time budget of 20 ms as defined by requirement 7. Requirement 3 states that only when the safety switch is triggered shall both feet be able to detach from the ground. To facilitate this during the active gait phase, a communication link needs to be present between both shoes for them to notify

each other once they are disconnected from the ground. This shoe-locking signal then prevents the shoe remaining on the ground from releasing accidentally and overwrites any outputs of the control algorithm.

3) **MSU:** The magnet and sensor unit is responsible for measuring all relevant states of the human foot, such that the critical gait phases can be differentiated by the state estimator. It is also responsible for giving the prototype the ability to attach to the ground via two electromagnets per shoe.

C. Subsystem Design

The SCU and MSU hardware schematic describing the system architecture and images of these subsystems can be seen in Figure 3. The following list walks through each block of the SCU schematic and explains its design in detail:

1) **12 V Input from PSU:** As a reliable solution complying with all requirements necessary to board the parabolic flight, a low profile *Wanptek DPS3010U* laboratory power supply, connected to an *Omnicharge Omni 20+* power bank via its AC output, was used as the PSU. The power supply was set such that it provides the necessary 12 V output, and its power button can be used as a switch to release the footwear from the ground in an emergency.
2) **5 V DC-DC Converter:** A *Traco Power TSR 2-2450* DC-DC converter is used to step the voltage down from 12 to 5 V for the logic system. At its input, a 100 µF capacitor is placed to filter possible fast changes in current when the electromagnets are turned on and off further down the electrical system.
3) **Microcontrollers:** A set of two different microcontrollers is used in the SCU to allow for maximal versatility in the system and to be prepared for multiple different modes of operation. For high-performance tasks, a *Teensy 4.1* development board equipped with an *ARM-Cortex-M7* is used. It is connected via UART to an *ESP32*. The latter board gives the system wireless capabilities and the ability to offload computational simple but time-intensive tasks, such as reading the digital sensors of the MSU. The *ARM-Cortex-M7* is used to sample the analog sensors of the MSU at 12-bit resolution via its ADCs. The remaining tasks of the microcontrollers are to actuate the magnets using two GPIO pins, to control the audiovisual system, and save all data to a storage device.
4) **Audiovisual System:** LEDs of different colors and a buzzer are used to communicate the system states to the user.

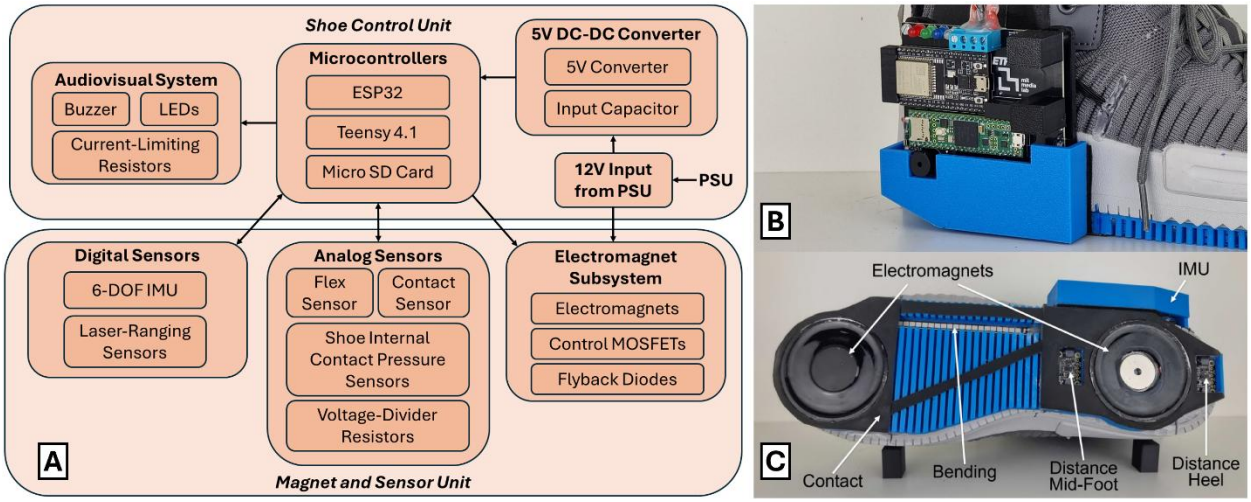

Figure 3: A) SCU and MSU hardware schematic, B) Close-up view of SCU, C) Close-up view of MSU

The components of the MSU are integrated into a 3D-printed flexible sole made from TPU. The following list walks through each block of the MSU section, seen in Figure 3a, and explains its purpose, components, and design:

1) **Electromagnet Subsystem:** The electromagnet subsystem is controlled via two GPIO pins, by changing the voltage at the gate of a transistor. This makes the actuation practically instantaneous when compared to the time constants of the human gait. When opened, the electromagnet is directly connected to the 12 V input voltage originating from the PSU, which provides the necessary current. The input and output of each magnet are connected to a flyback diode to protect the circuit from voltage spikes when the electromagnet is turned off due to the inductive energy stored in the windings. Electromagnets of the *WF-P70/9* type are used, due to their flat shape, good performance, low cost, and wide availability. Each magnet was tested to provide 250 N of stiction force to a

ferromagnetic plate. The heel electromagnet's core is replaced by a neodymium magnet and this characteristic is used in the sensor-based state machine control algorithm discussed in the control algorithm section of this paper.

2) **Analog Sensors:** Five analog sensors are integrated into the MSU: A flex sensor measuring the bending of the foot's sole, a sensor in the front of the foot measuring ground contact, and three textile-based piezoresistive sensors, inspired by current research, mounted on the inside of the shoe to get the contact pressure profile of the foot[9,22,23,24]. All sensors are read by the integrated ADCs of the *Teensy 4.1* microcontroller using voltage dividers. The textile sensors comprise four initial components: flexible silicone wire, conductive thread, piezoresistive fabric, and conductive cloth. Figure 4a shows the parts laid out such that the layers are stacked from left to right. When pressure is applied, the two conductive layers press the piezoresistive fabric in the middle together, thereby changing the resistance between both connected wires. The sensitivity of the sensor can be tuned here by adding multiple piezoresistive layers, which increases the resistance between the conductive wires. The final system uses two layers of piezoresistive material such that resistance is not too low when the maximum force expected is applied. The fabric sensors are mounted inside of the shoe as seen in Figure 4c.

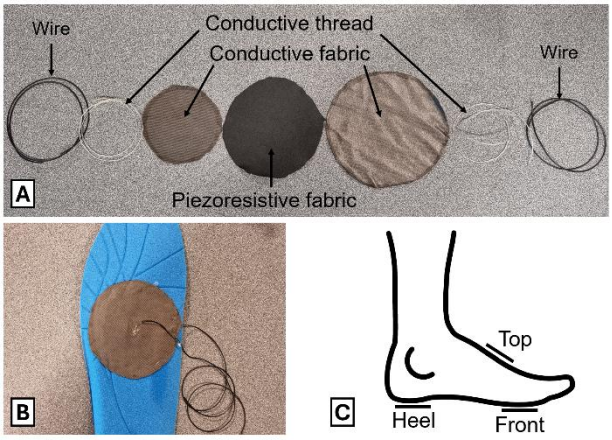

Figure 4: A) Textile contact pressure sensor assembly, B) Front sensor on shoe insole, C) Sensor placements

3) **Digital Sensors:** Three digital sensors are integrated into the system: Two *Adafruit VL53L4CD* laser ranging time of flight distance sensors and one *Adafruit ISM330DHCX* IMU. On Earth, accelerometers are often used to determine the orientation of an object in 3D space, which becomes impossible in microgravity due to the lack of acceleration downwards. Gyros can be used as an alternative but are subject to drift issues. For this reason, two laser ranging distance sensors are implemented instead of one, such that the angle of the foot can be determined by knowing the mounting distance between the two ranging sensors. The IMU can nevertheless provide detailed measurements in the dynamic phases of the gait cycle due to the rapid changes in velocity and angular motion. The distance sensors have a usable range between 1 mm and 1.3 m. The chosen IMU possesses three linear accelerometers and three gyroscopes to measure the acceleration and angular velocities of all six degrees of freedom in 3D-space. The maximum sampling rate of the laser ranging sensors achieved during testing was 200 Hz. These sensors are by far the most significant bottleneck in the embedded system, which needs to be considered in the system design and software.

D. Control Problem

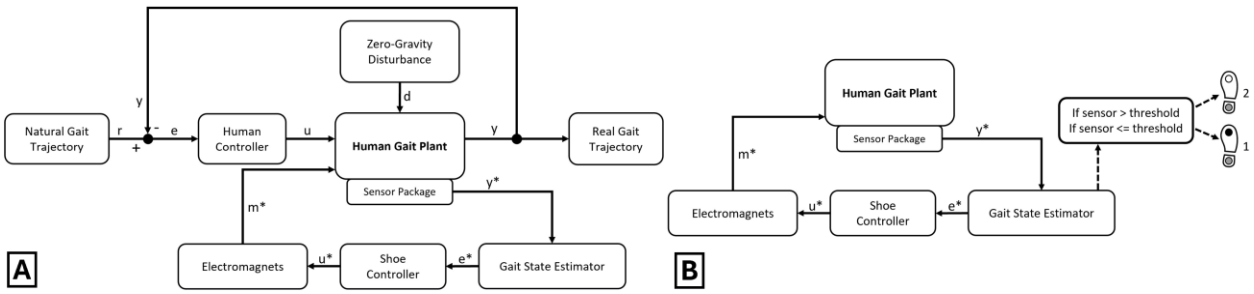

Figure 5: A) Control problem schematic, B) Sensor-based state machine control algorithm schematic

While walking, humans internally form a motion plan using an internal model of walking contact dynamics for applying proper torques for movement[25,26]. In the control diagram, this is labelled "Natural Gait Trajectory". This plan is modified by disturbances from reality experienced in the true dynamics, such as uneven speeds, unintended forces, and obstacles. The "Human Controller" block represents the closed loop feedback behavior the human body applies to maintain stable walking.

Microgravity significantly alters the "Human Gait Plant", removing the gravitational terms from the dynamics. The loss of gravity has a most consequential result: loss of the zero-velocity contact constraint from gravity and friction. With gravity and friction, the dynamics resemble an inverted pendulum[27,28]. Without constraint, the dynamics become that of a free rigid body, and the human no longer has the means to walk via controlled contact. This becomes a complete mismatch from the human's internal model of walking, and the solution space of stable gaits becomes empty. To make walking locomotion again possible in the microgravity environment, this work proposes the addition of a wearable actuation system that controls the strength and timing of the zero-velocity constraint of the stance foot to the floor. While this does not recover gravity, it does recover the zero-velocity contact constraint normally imposed by gravity and friction. We hypothesize this to be adequate for establishing the inverted pendulum, like dynamics of walking for human motion planning and control[27,28].

We aim to estimate the state of the human based on a series of sensors and use this estimate to control the contact constraint via electromagnets. The new shoe control loop consists of the following four sections:

1) **Sensor Package:** This set of sensors takes measurements pertaining to variables defining the current gait state, which includes the position, orientation, and associated velocities and accelerations. These measurements are fed into the state estimator. The measurement noise is sufficiently low such that no filtering was required. The aim is to create a detailed digital representation of human locomotion to be used in the next step.
2) **Gait State Estimator:** This stage uses the measurements gathered by the sensor package to estimate the current state in the gait cycle. In this project, the state of gait is discrete, classified to the three relevant gait phases as defined earlier in this work: heel-disconnected, fully-disconnected, and fully-connected. The output of the gait state estimator is then passed on to the controller.
3) **Shoe Controller:** Using the estimated gait state, the shoe controller applies the appropriate control law depending on the state. The control input is current, which turns on and off the electromagnets. The control of these electromagnets is performed open loop, which we have deemed sufficient as we mainly care about applying or removing the contact constraint to the floor.
4) **Electromagnets:** Once the control input signal has been passed through the embedded system and the magnets are powered on in the correct configuration, an attaching force between the ground and the shoes is generated. This creates the contact constraint with the floor in sync with the gait cycle, facilitating walking dynamics for the human.

Due to the complex interaction between the human plant and the electromagnetic shoe plant, estimation and control is difficult: the footwear is constantly attempting to guess where the human is in the gait cycle and anticipate the next phase of walking. Especially if the person loses their footing, or if the contact constraint was not well applied, the sequence of gait phases is often nondeterministic and difficult to solve using conventional state machine methods.

E. Control Algorithms

This paper investigates two methods to solve the control problem at hand: a sensor-based state machine and a neural network approach[25,26]. The state machine approach is commonly used for wearable robots such as exoskeletons and prostheses. However, we have found that the mode schedule applied in walking is harder to capture in microgravity, as any mistake in controlling the contact constraints is unforgiving relative to gravity. As a result, we created a data-driven neural network state estimator that acts as a measurement – state probability distribution and is therefore not dependent on hard-coded phases of walking[26]. We compare each of these methods in this work.

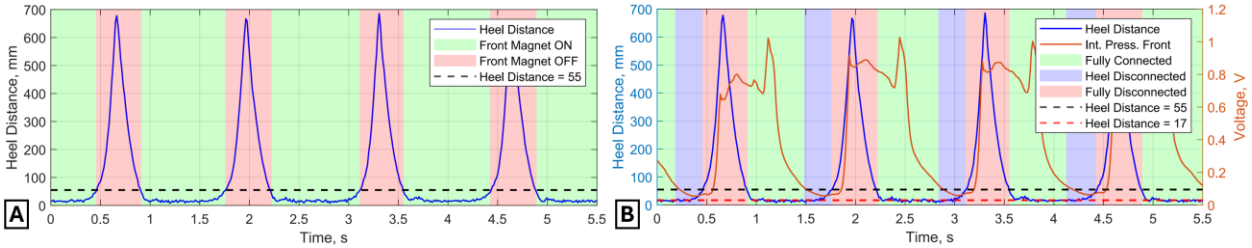

Figure 6: A) Heel distance sensor output segmented using a sensor-based state machine, B) Heel distance and front internal pressure sensor output segmented using a neural network control approach

The sensor-based state machine method emphasizes simplicity, by using direct measurements and a predetermined sequence of possible states to estimate the gait phase. The first simplification is to break the three introduced gait

phases down into only two: front electromagnet on and front electromagnet off. Meanwhile, the heel magnet is applied in a passive arrangement as a lightly magnetized permanent magnet by exchanging the electromagnet core with a neodymium magnet. This permanently attaches the heel of each foot to the ferromagnetic surface with a small force. The system is designed such that the heel is attached with only 15 N, equivalent to 1.5 kg on Earth.

The natural gait cycle begins with the foot completely connected to the ground. The body then shifts slightly upwards and forward by lifting the heel, disconnecting the heel from the floor. Once it is disconnected, the angle between the flat surface of the back of the foot's sole and the ground increases. The sensor package detects this motion, and when a predefined threshold is reached, the front electromagnet is turned off to release the foot fully, as shown in Figure 5b. Once the foot has completed the swing phase and returns to the ground, the system detects the approach, and the front magnet is turned on to attach again. In the final iteration, the heel laser ranging distance sensor at the back of the foot is used to determine the change in gait state, as plotted in Figure 6a.

A neural network is used in the second method as a state estimator, which takes the live sensor readings and their derivatives as an input and outputs the likelihood of each of the three possible gait phase scenarios. The controller is then able to choose the result with the highest possibility and actuate the electromagnets, as shown in Figure 7b.

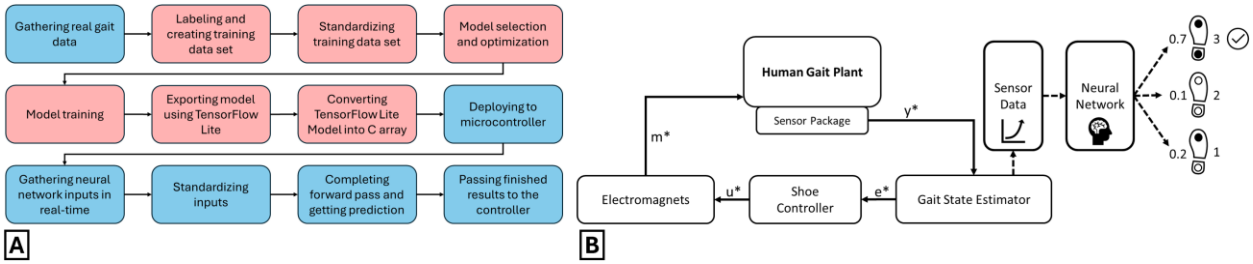

Figure 7: A) Machine learning pipeline, B) Neural network state estimator control algorithm schematic

The network was trained in a conventional supervised learning arrangement and integrated into our edge system using the *TensorFlow Lite Micro* library for real-time inference[29,30,31,32].

As a caveat, only gait data created in standard gravity was used to train, benchmark, and deploy the neural network state estimator. The main objective of this approach was to understand if this estimation and control method is viable for real-time use with the designed hardware. To achieve this in microgravity, two parabolic flights would have been necessary: an initial one for gathering the training data sets and a second one for deploying the finished models, with time for data analysis, training, and further testing in-between. This was not possible in the scope of this project, so gait data was gathered in gravity on Earth, where the readings are different, but the neural networks' ability to differentiate between the relevant gait phases can be proven by multiple real-time tests. Figure 7a visualizes the full supervised machine learning pipeline of the neural network state estimator, starting with the initial gathering of actual gait data and ending with the final model deployed on a microcontroller predicting the correct gait phase in real-time.

IV. Testing, Evaluation and Discussion

F. Parabolic Flight Testing

This test was conducted in cooperation with the *MIT Space Exploration Initiative* and the *Zero-Gravity Corporation*. Before the flight, an extensive hardware and documentation safety review process took place.

This test aimed to gather knowledge and data on the system's behavior and performance in a microgravity environment, while using the sensor-based state machine control method. The planned flight profile consisted of 20 parabolas with three different gravity settings: one parabola flown emulates the gravitational acceleration on Mars of 3.71 m/s^2, three emulating Luna-gravity of 1.62 m/s^2, and 16 in full weightlessness. Figure 8b shows the total acceleration data gathered by an onboard IMU, kindly provided by the *MIT Space Exploration Initiative*, visualizing the low- and hyper-gravity phases of the first ten conducted parabolas during flight.

The test setup used on board the plane consisted of two square ferromagnetic steel base plates, each measuring 60 by 60 cm with a thickness of 1.27 cm, mounted to the ground with a 30 cm gap between them, as seen in Figure 8d.

The prototype was mounted as seen in Figures 8a and 8c, with the 12 V power supply attached to the upper left leg and the power bank on chest height under the right arm. The wiring between the subsystems was guided via *Velcro* strips attached to the flight suit. The tests were documented via two cameras, one mounted on the rear steel plate and another attached to the user's chest.

The procedure of each gait test conducted during the flight started with the researcher laying with the back flat on the ground, as pictured in Figure 8c, for the hyper-gravity phase of each parabola. Once the transition to the lower gravity state has finished, the experimenter used the feet attached to the base plate to rotate upward into an upright position. Once stability has been achieved in the upright position, small steps are taken forward, until the edge of the first steel base plate has been reached, as seen in Figure 8a. To move to the next plate, a large step is taken. Small steps are used to rotate around here, and the gait test continues as before until the starting position is reached. This walking pattern could be achieved within the time available during each low-gravity phase of 20-30 s. An example data set of the small steps taken during the gait tests in microgravity can be seen in Figure 9.

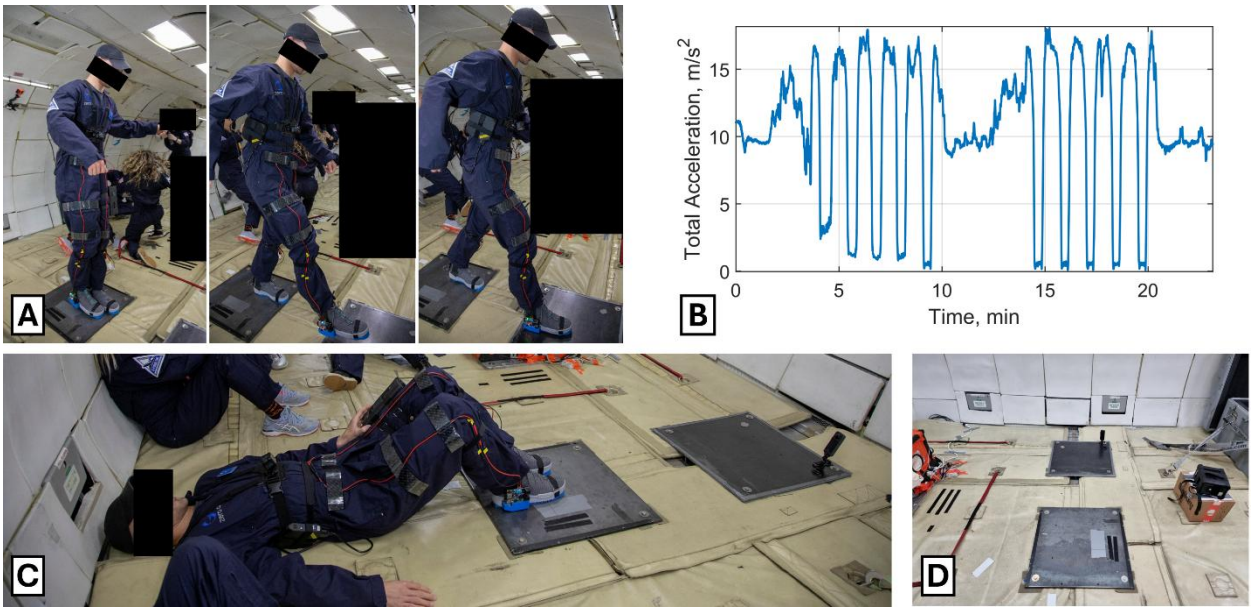

Figure 8: A) Gait tests in microgravity, B) Total acceleration during the first 10 parabolas, C) Hyper-gravity phase brace position, D) Test setup with ferromagnetic plates; 8a and 8c provided by *Zero-Gravity Corporation*

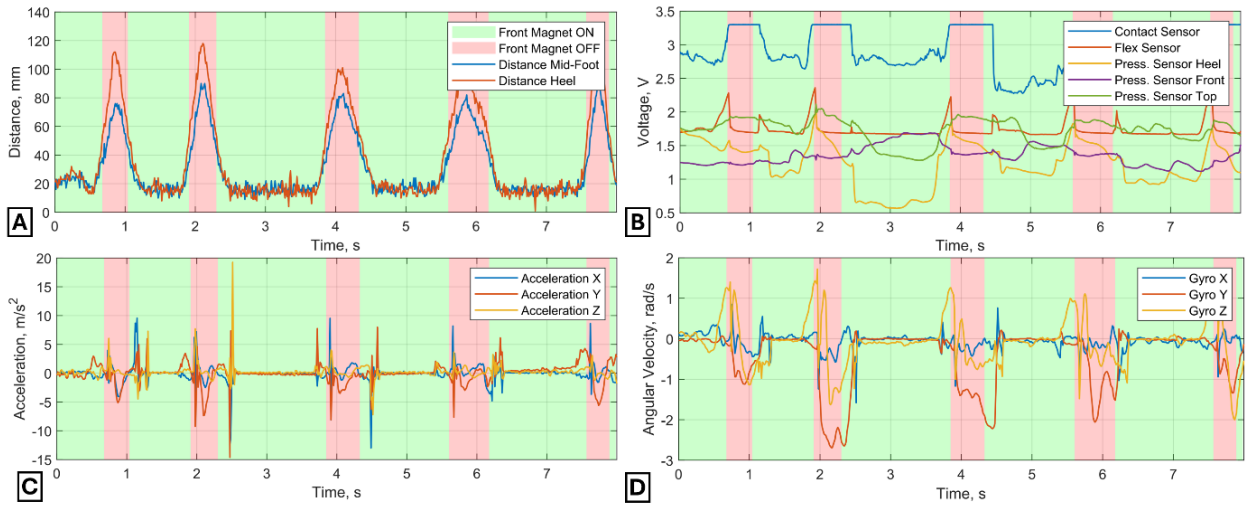

Figure 9: Gait sensor data gathered in microgravity: A) Distance sensors, B) Analog sensors, C) Acceleration measurements IMU, D) Gyroscope measurements IMU

Out of all measurements, the laser-ranging distance sensors visualize the foot's gait movement in the simplest way. When beginning a gait cycle, the heel starts to lift from the ground, increasing the distance from it and once the foot lifts off entirely and the maximum distance value can be seen. Then the foot swings around, moves down, and connects to the ground again. This creates a profile of continuous peaks over the course of a gait test.

The IMUs z-axis gyroscope measures the rotational velocity around the ankle's main rotation axis. This sensor can, therefore, gather data regarding the foots swing motion. At the beginning of the gait cycle, the foot is connected to the ground, with no rotational velocity present. Then the heel lifts off, while the ankle starts to rotate backward, creating positive readings. Once the foot is fully released from the ground, it rotates forward to position itself to contact the ground again, changing the sign of the sensor value. This creates the swing motion seen, with a positive and negative section.

The flex sensor's behavior represents the bending of the shoe sole. Its dynamics are mainly confined to the first section of the gait cycle, where the heel starts to lift off, while the front is still connected to the ground. Only at this point in the cycle is significant bending taking place in the sole. Once the shoe lifts off entirely, its shape snaps back to its original flat state, returning the sensor to its steady state value.

The internal heel pressure sensor's output is low when a force is applied and high otherwise. At the beginning of the gait cycle, when the heel leaves the ground, the pressure on this sensor reduces, increasing the read value. Once the foot touches the ground, pressure on it returns, lowering the sensor value. In contrast to the other three sensors presented in this chapter, this sensor's behavior changes drastically when deployed in weightlessness compared to an environment with gravity. The Luna measurements give much more useful sensor readings than in microgravity. This is due to the fundamental changes in the gait experience. In weightlessness, the human body constantly wants to move upwards when standing on the ground due to even the slightest contact force between the foot and the floor pushing one's body away. As a result, when wearing the designed footwear, the user always tries to anchor himself by pushing the front part of the foot upwards against the top of the shoe to keep the heel down, just like astronauts do when putting their feet into holding straps. This is done with minimal effort compared to the usual gravitational force, lowering the sensor's readings and making it less prominent. The analysis of this data highlights the importance of the design of the internal pressure sensors and making them sensitive enough to pick up the wanted dynamics.

Through the data analysis and test experience, the following conclusions, observations, and recommendations for improvements can be made regarding the parabolic flight test in terms of the user experience and technical aspects:

1) **General performance:** The system enabled its main functionality of allowing walking in microgravity well. It was possible to detach and re-attach the shoes easily solely via the user's natural gait motions. The tests always started with the experimenter lying on his back for the hyper-gravity phase of the parabolic flight. Once the low gravity phase has begun, the user could switch to an upright position, by simply using the attached feet to rotate the body around the ankles, via a sitting position. The magnets proved to be strong enough to facilitate this motion, and the rubber surface on the sole of the shoe prevented any slip. Once upright, walking could commence after a short period of standing still. It can be noted that this test procedure naturally also included the verification of the other use case scenarios such as standing, sitting, and the transitions in between.
2) **Missing shoe-locking feature and weak heel permanent magnet:** Due to the strict rules regarding EM wave emitting devices on the parabolic flight to prevent interference with other experiments, no wireless communication was enabled while testing the system. Therefore, the shoe-locking feature, described in the system overview and interfaces section of this work, facilitated through wireless communication between the two shoes, was disabled during the tests. Furthermore, the rear permanent magnet, designed to keep the heel attached until the user releases it, turned out to be not strong enough, giving the system the tendency to release too quickly. This allowed the situation that during the swing phase of the gait cycle, the heel of the attached foot was released prematurely and sent the signal to the control system to release the foot fully. This made the user completely lose contact with the ground. In the final configuration, this would be prevented by the activated shoe-locking feature.
3) **Test setup:** Due to the mounting points in the plane and components available, there was a large gap between the ferromagnetic base plates, as seen in Figure 8d. This gap led to gait with varying step size and makes the data set less uniform and the analysis harder. A setup allowing for a more standardized data set to be created would have been preferable during this state of the development process.
4) **Toe strap addition and top force sensor:** Due to the necessity to give the user's toes a place to push up against, the fabric of the used shoes was strengthened by adding a strap at this location, as seen in Figure 8a and 8c. This improved the shoe's fit significantly and gave more stability in weightlessness but prevented pressure from being projected onto the top force sensor in the shoe. This impacted the sensor readings negatively. The strap should have been placed right above said sensor, such that the pressure placed onto the strap could have been detected and measured more clearly.
5) **Sensor performance:** The sensors need a tailored solution to improve consistency. On the digital sensor side, the IMU precision needs to be adjusted in software to be more sensitive, and the analog internal pressure sensors need

to be attached better to the user to pick up the desired signals. The latter can be solved by tightening the shoe further and by inserting a harder background material to offer a better foundation to press against.

6) **Testing procedure variety:** During the parabolic flight test, the same gait pattern was followed during all tests to give a good understanding of the system in a realistic environment. Nonetheless, this created data sets with large variances due to changes in the physical actions taken e.g., small steps forward, large steps over the gap between the two base plates, and small steps while turning around. From the system and sensor side, more simplified scenarios, such as walking in the same spot with small reproducible steps for a few parabolas, would have created cleaner data sets and given a larger sample of the system behavior in the same scenario.

G. Ground Testing

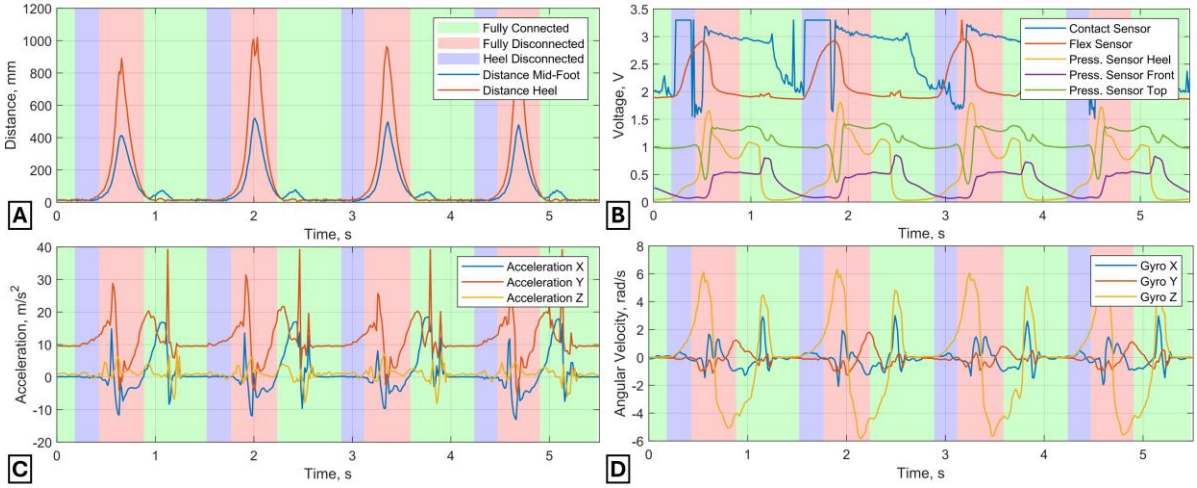

Figure 10: Gait sensor data gathered in earth gravity: A) Distance sensors, B) Analog sensors, C) Acceleration measurements IMU, D) Gyroscope measurements IMU

During the ground testing campaign, the objective was to gather data suitable for training sets for machine learning applications and test the final configuration's functionality, including the telemetry network and neural network control algorithm under standard gravity. This represents the ideal case for the sensor array to acquire high quality readings due to the consistent and faster walking pace as well as larger forces on the internal pressure sensors because of gravity. At the beginning and end of each walking test, the experimenter stands still for a few seconds so the system can gather data for the neural network to be able to classify the standing scenario correctly. Figure 10 shows an example of data gathered in standard-gravity during a periodic gait pattern with constant steps. All sensors show the expected behavior, and the separation between the different gait phases can clearly be seen. These data sets are the foundation for the training of the neural network control algorithm, as discussed in a later section.

The only fault found in the prototype during the ground testing campaign was an apparent failure of the right shoe's flex sensor due to a faulty soldering connection, which could be repaired easily.

H. Limit Cycle Analysis and Sensor Selection

Now that an extensive amount of testing data in different gravity scenarios has been gathered, it needs to be decided which sensors are viable for detecting the different gait phases accurately and reliably. Besides the actual sensor reading, its derivative is essential for many control and classification approaches. For the classification problem at hand, it is important that all sensors used show clear uniqueness at all points during the gait cycle, such that the correct phases can be detected reliably. A limit cycle can be used to visualize this characteristic. Here, the sensor output is plotted on the x-axis, and its derivative is on the y-axis. Ideally, the graph should

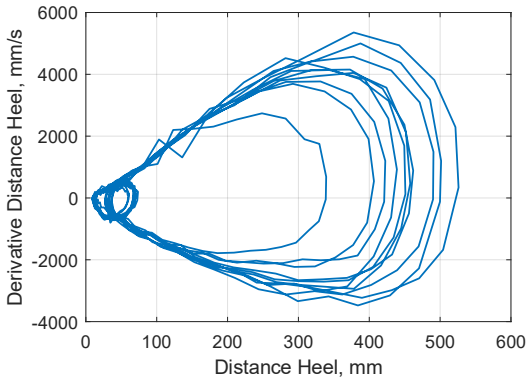

Figure 11: Limit cycle of mid-foot distance sensor during ground testing in standard-gravity

show the path of a shape, which is reliably traced across each gait cycle and shows uniqueness at each point of the plot. The limit cycle of the mid-foot distance sensor during ground testing can be seen in Figure 11 as an example. Considering all limit cycles, it was seen that most sensors provide suitable readings and derivatives describing the gait dynamics. Exceptions are the x-y-axis gyroscopes, with only the z-axis measuring the relevant rotation around the ankle, and all accelerometers, due to inconsistent readings.

I. Labeling of Training Data

At the beginning of any supervised machine learning pipeline, it is necessary to acquire high quality labeled training data sets[31,32]. The training data used in this project was taken during the ground testing campaign. The next step is to find an efficient way to label the testing data accurately. To achieve this, an algorithm is needed that takes in sensor data and detects the correct gait phase of each data point. It must then label said entries as fully-connected, heel-disconnected, or fully-disconnected, corresponding with the gait phase, as seen in the case of the heel distance and front pressure sensor in Figure 6b.

The proposed algorithm separates the different phases the following way: The fully-disconnected phase is determined with the same logic as used in the sensor-based state machine, by deciding on a threshold on the heel distance sensor, above which we want to disconnect the foot entirely. This value was set to 55 mm during the parabolic flight and proved to be in the correct range regarding the user experience. The difficult task is to determine the transition point between the fully-connected and heel-disconnected phases, in that the controller needs to release the back of the foot right before the natural gait movement would lift it up. To find this point, the heel distance sensor can show us the exact moment the first motion upwards is detected, using an empirically set distance threshold of 17 mm. Having an approximately constant gait cycle, the algorithm can choose a data point a few samples before the heel-off is detected and decide to label the data set such the heel electromagnet gets released at this point. In the algorithm, the heel releases 200 ms before the user wants to lift it up. Once this point is found, the non-labeled data to the left and right can be marked as fully-connected and heel-disconnected respectively, until the already labeled fully-disconnected set is reached. The thresholds used in the algorithm are marked in Figure 6b.

Even though the heel sensor is used to find the separation point between the fully-connected and heel-disconnected phase, it is not able to detect it directly in real-time, due to the nature of the labeling algorithm. When the sole is flat on the ground the heel distance sensor measures a constant value and mainly the internal pressure sensors are in their dynamic phase. The neural network takes multiple sensor readings as inputs to cover such blind spots and offers the ability to play to the extensive sensor array's strength.

With this algorithm at hand, a training data set consisting of 180 steps, which are described by over 18000 individual data points, is labeled and used in the next steps of the machine learning pipeline. A labeled example data set of all relevant sensors of the MSU can be seen in Figure 10.

J. Model Selection, Optimization, and Performance

Once the labeled training data set has been acquired, a fitting machine-learning model needs to be found. In the case of a neural network, this entails defining its structure, activation functions, and possibly other hyper-parameters. The computational requirements, due to the use of low-powered microcontrollers, only allow for small neural networks to keep the time needed for the forward pass within a few milliseconds[29].

A variety of different models were investigated. As a benchmark for model performance, validation and testing accuracy is used.

The fully labeled data set is split up into training, testing, and validation subsets with a 70 %, 15 %, and 15 % split respectively, according to standard machine learning practices and iteration[31,32]. The validation accuracy plotted against the number of epochs of a small selection of the model approaches investigated can be seen in Figure 12a. This includes the baseline neural network, and models following a deeper and wider network structure, as well as different activation functions.

Due to the similar performance of the investigated models, reaching 98 % of validation accuracy consistently, no extensive optimization was necessary. The limiting factor preventing higher accuracy seems model-independent and likely due to the labeling algorithm not choosing a perfectly defined point to separate the fully-connected and heel-disconnected states. The final model implements four fully connected hidden layers with 128, 64, 32, and 16 neurons respectively and the standard ReLU activation function. This represents a combination of a deep and wide approach. The output layer uses a Softmax activation function to ensure that the output represents a proper probability distribution of the three possible gait phases and sums to one. It is desirable to keep the machine learning model able to generalize with new data such that it can react well in unseen situations. All networks trained include dropout layers

with a 30 % dropout rate during training and early stopping is used at the peak of the validation accuracy, both to prevent over-fitting to the training data.

The final model investigated inputs all sensors found to be suitable via their limit cycles, which includes 8 direct sensor readings, the calculated foot angle, and the derivatives of the three internal pressure sensors, totaling 12 inputs. As benchmarks for neural network performance, the already introduced training and validation errors are used and are extended by the relevant ROC plots and normalized confusion matrices.

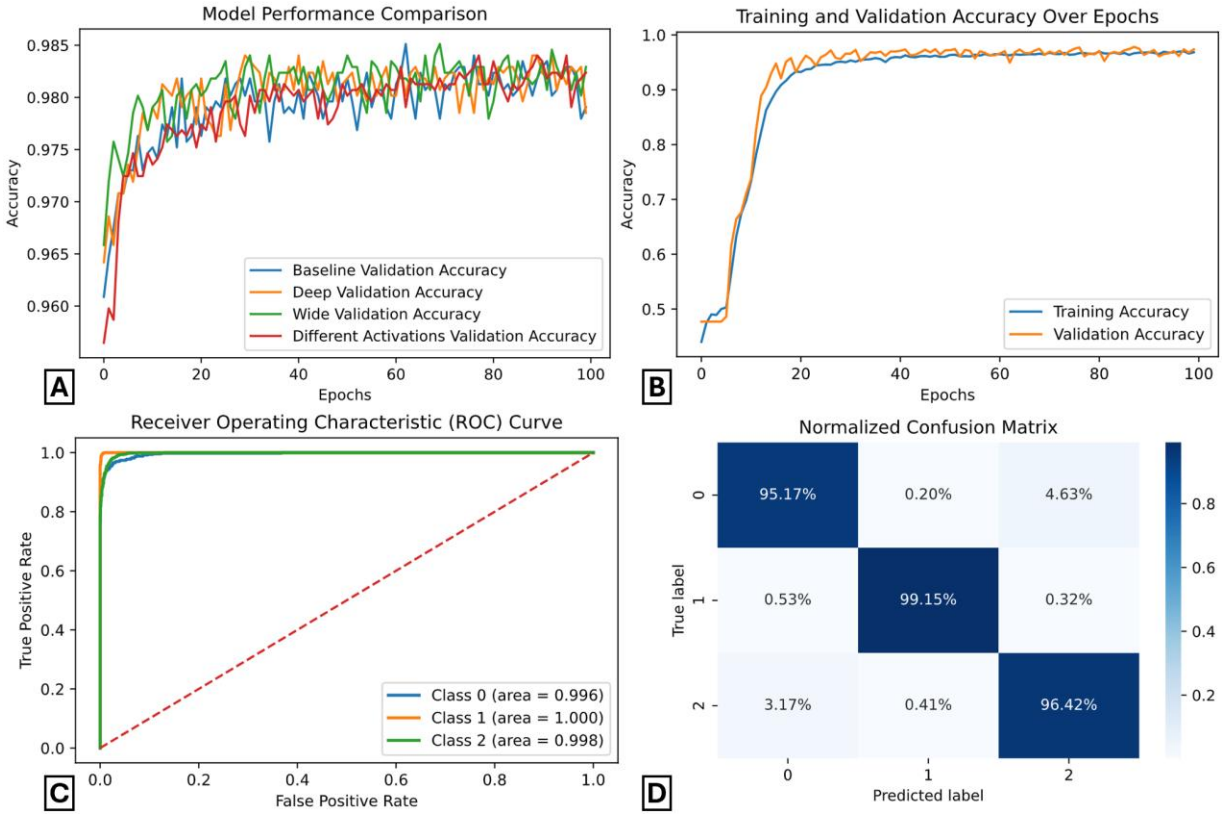

Figure 12: A) Validation accuracy over epochs of investigated models, B) Training and validation accuracy over epochs of final model, C) ROC curve of final model, D) Normalized confusion matrix of final model

Figures 12b and 12c show the training and validation accuracies as well as the ROC curve of the final model, using the all-sensor setup. The relevant normalized confusion matrix can be found in Figure 12d, with class 0 representing the heel-disconnected, class 1 the fully-disconnected, and class 2 the fully-connected gait cycle phase. The model delivers between 95 and 99 % accuracy in the three classes. The ROC curve also shows the good performance of the model, with the graph being close to a 90 degree angle in the upper left corner, approaching the ideal case. The few misclassifications remaining, totaling to 2 % of the validation data set, predominantly originate from the neural network detecting a state change slightly sooner or later than the labeling algorithm, as discussed in the next section.

K. Deployment and Real-Time Behavior

Until now, the models have only been trained, tested, and bench-marked with a labeled data set originating from the same series of gait tests. It is important to gather data regarding the generalized performance of the network when it is used in real-time, receiving completely new data the model has not yet seen. Taking the shoes on and off can move sensors slightly, due to the flexible nature of the fabric and TPU sole. This and many more areas can introduce slight deviations in the sensor readings, making the ability to generalize even more critical to the network. As the concluding part of the ground testing campaign, a gait test with the final configuration and a running neural network was conducted, gathering real-time performance data. Due to simplicity and having a more intuitive overview of the model behavior, a model only trained on two sensor readings was deployed, namely the heel distance and heel internal pressure sensor. With only two sensors feeding into the neural network, the system can be tested and debugged much

more easily than using the full spectrum of the available sensors. The goal of this test is to gain knowledge regarding the difference in accuracy calculated during the training of the model and the final deployment.

Figure 13 shows the real-time predicted labels, overlapped with the labels given by the labeling algorithm. The expected accuracy for this dual sensor model is 90 %, with the real-time test showing 87 %. This means that the deployed system performs close to 97 % as expected, making the results gathered during the training and benchmarking process significant and a reliable estimation.

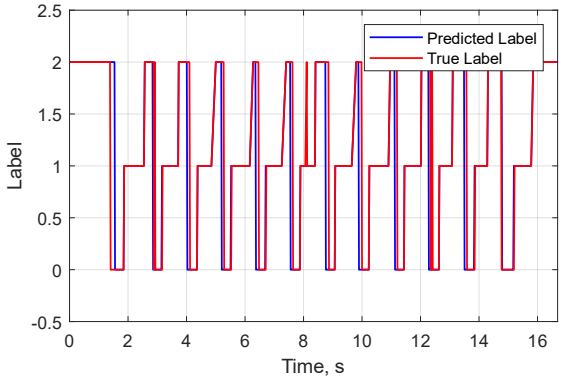

Figure 13: Comparison true labels with real-time labeling of neural network

Figure 13 also confirms the theory that most misclassifications predominantly originate from the neural network detecting a state change slightly sooner or later than the labeling algorithm due to the two graphs generally only misaligning during transitions. Only at 2.9, 8.1, and 12.4 seconds in the example data set can proper misclassifications be seen, which are not just due to an early or late system response. The high sampling rate should keep their effect on the user experience minimal and the shoe-locking feature will guarantee attachment in any case.

L. PSU Power Analysis and Improvements

When considering deploying a future iteration of the proposed system on a space mission, power consumption becomes one of the main issues. This project aims to provide a first power analysis and give recommendations on how to limit the necessary consumption. The current drawn by a single shoe with zero, one, and two active magnets is 0.26 A, 1.41 A, and 2.54 A respectively. This means one magnet needs 1.14 A on average with the prototype needing an additional 0.26 A for the embedded system. The components run on a voltage of 12 V, leading to a power consumption of 13.68 W per magnet and 3.12 W for the rest of the electronics. When the user is standing still, all four magnets are attached to the ground, requiring the system to use 57.84 W. During the walking phase, the data shows that averaging over time, the power consumption can be estimated as being equivalent to having one magnet powered on constantly per foot, which decreases the power consumption to 30.48 W.

The obvious choice is to optimize the electromagnets, being the components with the highest power consumption by an order of magnitude. The most promising solution would be to replace the standard electromagnets with custom-made electropermanent magnets[33]. These magnets act just like permanent magnets, but with the ability to turn off their magnetic field, requiring a coil to be only pulsed when its corresponding magnet is to be released. This is achieved by combining a magnetically soft and hard material in a magnetic loop and placing a wire around the soft magnetic material to give the option of creating short pulses of strong magnetic fields. This can be used to reverse the magnetic polarization in the soft magnetic material, changing the path the flux takes. This either confines the flux to the magnetic loop itself or guides it on the outside making it possible to attach an external ferromagnetic object[34].

To assess the actual potential this improvement could bring, the energy needed by EPMs for the application present needs to be estimated. As the magnetically soft component, AlNiCo magnets are used. To approximate the energy necessary to flip the magnetic field of this alloy, one can multiply the product of the volume of the magnet, its coercivity, and its magnetic flux density by two. This equation assumes a rectangular BH-curve and no losses due to electrical resistance or in the pulsed power circuit[35]. The magnetic flux density B and the coercivity H for AlNiCo magnets can be assumed to be 1.2 T and 80 kA/m respectively[36]. The volume is estimated as a disc with a diameter of 2.5 cm and a thickness of 3 mm, according to the dimensions of the neodymium permanent magnets used in this project. Having all values available, the presented formula can be used, to estimate the required energy for one flip of the magnetic field to be 3.4 J, which includes a conservative loss factor of three.

When assuming a gait frequency of 1 Hz, according to the data gathered during the parabolic flight, four magnet actuations are necessary per second per shoe while walking with the current prototype. Averaging the energy need for the EPMs over time results in a constant power requirement of 13.6W. When compared to the power usage during active gait of 30.48W while using the traditional electromagnets integrated in this project, the EPM solution would offer a power reduction of over 45 %, when including the 3.12W needed for the embedded system. This would already offer a significant decrease in power usage, but the real savings come into play when no active gait is present: While standing still, no magnets need to actively change their magnetization, eliminating any power consumption besides the requirements for the embedded system in the EPM case, which represents a reduction in the power consumption

of 95 %. Arguably, astronauts are generally working in a more stationary way, making the impact of the EPMs even more significant and them possibly the key to the functional deployment of this technology.

V. Conclusion, Outlook, and Future Work

The intelligent electromagnetic footwear prototype developed under this project fulfills all main requirements as defined by this paper: On the safety side, the system successfully deploys a power supply unit, able to monitor the state of the integrated battery and supply the system over the required time of 30 min. The prototype implements a telemetry network that synchronizes both shoes, such that only one can release at a time, which always guarantees the required contact force of 400 N. The integrated control algorithms only use the natural gait dynamics of the user as inputs, measured by the system's sensor package, which allows for an effortless walking experience for the wearer, with no need to concentrate on the magnet actuation. All these functionalities are packed into a low-power and low-cost embedded system able to deliver a system response time of less than 20 ms, enabling fluent real-time user experience.

Both control algorithms investigated, a sensor-based state machine and a neural network approach, were tested extensively, revealing their strengths and areas for improvement. The sensor-based state machine method was successfully deployed on a parabolic flight, allowing for the opportunity to gather extensive insight into the system's performance and user experience in an operational microgravity environment. The neural network approach was trained and tested during a ground testing campaign, allowing the functionality to be shown in a laboratory environment. Both control methods proved to be valid options for an improved version of the system, with only minimal adjustments necessary. This report recommends the sensor-based state machine approach due to its simplicity and the reduction in possible system failure modes coming with it. The sensor signals look to be sufficiently simple and consistent to not warrant the need for the neural network, at least in the situations we explored.

The extensive testing campaign proved the feasibility of the proposed concept and showed the value it could bring to the future of locomotion in microgravity. It provides an extensive knowledge base for future iterations of the system and an assessment of the user experience, able to highlight areas of improvement and future research.

The success of this project with the developed prototype and the proof of concept, allows us to envision a future deployment of the system on an extended mission in space. The following work packages highlight the areas to be investigated to improve the design and to allow the further progression of the project:

1) **EPM integration and further testing:** Reducing the system's power consumption is key to making the concept deployable on a real mission, with electropermanent magnets offering an efficient and elegant improvement. We predict a possible reduction in power consumption by 45 % during active gait and even 95 % while the user is standing still or sitting when integrating this technology. This would be a fundamental improvement, enabling a multitude of positive design changes, such as reducing the size of the power supply system and making the prototype more comfortable for the user to wear. The knowledge gathered throughout this project would furthermore allow for a more condensed second prototype design. This could entail a reduction in the sensor array and embedded system, according to the needs of the final control design and integrating all PSU functionality into the shoes, removing the need for external cables and making wearing the system much more comfortable. This new prototype could undergo a second more focused microgravity testing campaign with an improved test setup, allowing for more continuous gait and the ability to switch between control methods while in flight.
2) **Design of magnetic walkways:** A topic not discussed in detail in this work is the design of the magnetic walkways for the system's deployment. The inherent restrictions on the design due to the potentially high launch cost of ferrous material into space lead to an exciting engineering challenge spanning many fields, such as material science (e.g., defining the thinnest and lightest magnetic material for the walkways) and structural design (e.g., percolating the magnetic substrate to make it lighter).
3) **Space architecture:** On a more artistic note, the impact of this new method of locomotion on the way habitable zones are designed for space missions could be investigated. The option of not only being able to use the floor to stand on, like on Earth, but also the walls and ceiling of a room can make fundamental changes in the current understanding of architecture and working in space possible.

Acknowledgments

We would like to express our gratitude to *Cody Paige*, *Sean Auffinger*, the *MIT Space Exploration Initiative*, and the *Zero-Gravity Corporation* for making the tests in microgravity possible and for providing flight data and pictures.

This work was primarily conducted as a master's thesis at the *Responsive Environments Group* at the *MIT Media Lab*, in collaboration with the *Sensory-Motor Systems Lab* at *ETH Zürich*[37].

References

[1] N. Adilov, P. Alexander, B. Cunningham, and N. Albertson, "An analysis of launch cost reductions for low earth orbit satellites," *Economics Bulletin*, vol. 42, no. 3, pp. 1561–1574, 2022.

[2] A. Ekblaw, A. Prosina, D. Newman, and J. Paradiso, "Space habitat reconfigurability: TESSERAE platform for self-aware assembly," in *Proc. 30th IAA Symp. Space Soc*, 2019.

[3] G. D. Valle, D. Litteken, and T. C. Jones, "Review of Habitable Softgoods Inflatable Design, Analysis, Testing, and Potential Space Applications," in *AIAA Scitech 2019 Forum*, Reston, Virginia: American Institute of Aeronautics and Astronautics, Jan. 2019. doi: 10.2514/6.2019-1018.

[4] Stanley Kubrick, United States. *2001: A Space Odyssey*, (1968).

[5] Naren Shankar, United States. *The Expanse*, (2015).

[6] D. D. Haddad, F. Ward, I. Wicaksono, and J. Paradiso, "Magnetic Space Grip Shoe.," *Wearable Technology for Space Exploration*, Sep. 2021.

[7] Y. A. Petrov, "Habitability of Spacecraft," *Foundations of Space Biology and Medicine: Space medicine and biotechnology*, vol. 3, p. 157, 1975.

[8] D. J. Newman, J. A. Hoffman, K. Bethke, J. A. Blaya, C. E. Carr, and B. Pitts, "An Astronaut 'Bio-Suit' System: Exploration-Class Missions," 2003. [Online]. Available: https://api.semanticscholar.org/CorpusID:146065320

[9] S. Payra, I. Wicaksono, J. Cherston, C. Honnet, V. Sumini, and J. A. Paradiso, "Feeling Through Spacesuits: Application of Space-Resilient E-Textiles to Enable Haptic Feedback on Pressurized Extravehicular Suits," in *2021 IEEE Aerospace Conference (50100)*, IEEE, Mar. 2021, pp. 1–12. doi: 10.1109/AERO50100.2021.9438515.

[10] I. Wicaksono, A. Shtarbanov, E. Ranade, R. Slater, D. Newman, and J. Paradiso, "Design, Development, and Testing of Peristaltic Suit: Active-Dynamic Compression and Physiological Sensing Intra-vehicular Activity Spacesuit for Cardiovascular Deconditioning," 2023.

[11] P. Lee *et al.*, "Astronaut smart glove: A human-machine interface for the exploration of the moon, mars, and beyond," 2020.

[12] A. Ekblaw *et al.*, "From UbiComp to Universe—Moving Pervasive Computing Research Into Space Applications," *IEEE Pervasive Comput*, vol. 22, no. 2, pp. 27–42, Apr. 2023, doi: 10.1109/MPRV.2023.3242667.

[13] R. J. Radus and W. G. Evans, "Apparatus responsive to direct quantities," Jun. 1959, *Google Patents*.

[14] J. J. Astleford and R. J. Radus, "The Zero Impedance Distribution Transformer," *IEEE Transactions on Power Apparatus and Systems*, vol. 83, no. 9, pp. 918–926, Sep. 1964, doi: 10.1109/TPAS.1964.4766092.

[15] A. W. Hanger, S. C. Harris, and A. A. Rosener, "Final analysis/design and prototype construction of a selected mobility and restraint device Final report," 1969.

[16] A. Rosener and A. Hanger, "The use of permanent magnets in zero-gravity mobility and restraint footwear concept," *IEEE Trans Magn*, vol. 6, no. 3, pp. 464–467, Sep. 1970, doi: 10.1109/TMAG.1970.1066852.

[17] E. B. Simonsen, *Contributions to the understanding of gait control*. University of Copenhagen Copenhagen, 2014.

[18] I. P. I. Pappas, M. R. Popovic, T. Keller, V. Dietz, and M. Morari, "A reliable gait phase detection system," *IEEE Transactions on Neural Systems and Rehabilitation Engineering*, vol. 9, no. 2, pp. 113–125, Jun. 2001, doi: 10.1109/7333.928571.

[19] F. Sylos-Labini, F. Lacquaniti, and Y. P. Ivanenko, "Human Locomotion under Reduced Gravity Conditions: Biomechanical and Neurophysiological Considerations," *Biomed Res Int*, vol. 2014, pp. 1–12, 2014, doi: 10.1155/2014/547242.

[20] Meng Chen, Bufu Huang, and Yangsheng Xu, "Intelligent shoes for abnormal gait detection," in *2008 IEEE International Conference on Robotics and Automation*, IEEE, May 2008, pp. 2019–2024. doi: 10.1109/ROBOT.2008.4543503.

[21] T. W. F. Mittlemeier and M. Morlock, "Pressure Distribution Measurements in Gait Analysis: Dependency on Measurement Frequency," in *39th Annual Meeting of the Orthopaedic Research Society*, San Francisco, Calif, 1993.

[22] I. Wicaksono *et al.*, "3DKnITS: Three-dimensional digital knitting of intelligent textile sensor for activity recognition and biomechanical monitoring," in *2022 44th Annual International Conference of the IEEE Engineering in Medicine & Biology Society (EMBC)*, 2022, pp. 2403–2409.

[23] Y. Luo, J. Zhu, K. Wu, C. Honnet, S. Mueller, and W. Matusik, "MagKnitic: Machine-knitted Passive and Interactive Haptic Textiles with Integrated Binary Sensing," in *Proceedings of the 36th Annual ACM Symposium on User Interface Software and Technology*, New York, NY, USA: ACM, Oct. 2023, pp. 1–13. doi: 10.1145/3586183.3606765.

[24] I. Mileti, S. Pasinetti, J. Taborri, F. Patanè, M. Lancini, and S. Rossi, "Realization and validation of a piezoresistive textile-based insole for gait-related measurements," in *2023 IEEE International Instrumentation and Measurement Technology Conference (I2MTC)*, IEEE, May 2023, pp. 1–6. doi: 10.1109/I2MTC53148.2023.10176102.

[25] A. H. Shultz, J. E. Mitchell, D. Truex, B. E. Lawson, E. Ledoux, and M. Goldfarb, "A walking controller for a powered ankle prosthesis," in *2014 36th Annual International Conference of the IEEE Engineering in Medicine and Biology Society*, IEEE, Aug. 2014, pp. 6203–6206. doi: 10.1109/EMBC.2014.6945046.

[26] H. Kim, D. Lee, J. Y. Maldonado-Contreras, S. Zhou, K. R. Herrin, and A. J. Young, "Mode-Unified Intent Estimation of a Robotic Prosthesis Using Deep-Learning," *IEEE Robot Autom Lett*, vol. 10, no. 4, pp. 3206–3213, Apr. 2025, doi: 10.1109/LRA.2025.3535186.

[27] A. D. Kuo, "The six determinants of gait and the inverted pendulum analogy: A dynamic walking perspective," *Hum Mov Sci*, vol. 26, no. 4, pp. 617–656, Aug. 2007, doi: 10.1016/j.humov.2007.04.003.

[28] G. Antoniak, T. Biswas, N. Cortes, S. Sikdar, C. Chun, and V. Bhandawat, "Spring-loaded inverted pendulum goes through two contraction-extension cycles during the single support phase of walking," *Biol Open*, Jan. 2019, doi: 10.1242/bio.043695.

[29] R. David *et al.*, "TensorFlow Lite Micro: Embedded Machine Learning for TinyML Systems," in *Proceedings of Machine Learning and Systems*, A. Smola, A. Dimakis, and I. Stoica, Eds., 2021, pp. 800–811. [Online]. Available: https://proceedings.mlsys.org/paper_files/paper/2021/file/6c44dc73014d66ba49b28d483a8f8b0d-Paper.pdf

[30] M. Abadi *et al.*, "TensorFlow: Large-Scale Machine Learning on Heterogeneous Distributed Systems," 2016. [Online]. Available: https://arxiv.org/abs/1603.04467

[31] E. Alpaydin, *Introduction to Machine Learning*, 4th ed. MIT Press, 2020.

[32] I. Goodfellow, Y. Bengio, and A. Courville, *Deep Learning*. MIT Press, 2016.

[33] "Human fly has magnetic sole," *Electrical Engineering*, vol. 82, no. 4, pp. 294–294, Apr. 1963, doi: 10.1109/EE.1963.6541068.

[34] A. Knaian, "Electropermanent magnetic connectors and actuators: devices and their application in programmable matter," Massachusetts Institute of Technology, Cambridge, MA, USA, 2010. [Online]. Available: http://hdl.handle.net/1721.1/60151

[35] A. E. Fitzgerald, C. Kingsley, and S. Umans, *Electric Machinery*. in Electrical Engineering Series. McGraw-Hill Companies,Incorporated, 2003. [Online]. Available: https://books.google.at/books?id=YBKk4kWSle0C

[36] Dexter Magnetic Technologies, "Alnico Properties Table and Curves," 2024. [Online]. Available: https://pdf.directindustry.com/pdf/dexter-magnetic-technologies/alnico-properties-table-curves/23025-427085.html

[37] S. Meyer, "Design and Control of Intelligent Electromagnetic Footwear for Space Applications," Unpublished master's thesis, Massachusetts Institute of Technology and Swiss Federal Institute of Technology Zurich, 2024.